Climate Dynamics (2025) 63:81
https://doi.org/10.1007/s00382-024-07574-8

ORIGINAL ARTICLE

A possible two-way feedback between El Niño–Southern Oscillation and Arctic stratospheric ozone

Hongwei Liu[1] · Fei Xie[1] · Yan Xia[1] · Jianping Li[2]

Received: 17 September 2024 / Accepted: 26 December 2024

Abstract
It is well established that the anomalous sea surface temperatures caused by the El Niño-Southern Oscillation (ENSO) can impact polar stratospheric ozone concentrations in 2–3 months. In recent years, the climatic impact of stratospheric ozone has received widespread attention. Some studies even suggest that Arctic stratospheric ozone (ASO) can affect the intensity of ENSO. So, is there a potential bidirectional feedback loop between ENSO and ASO? Based on observational and reanalysis data, this study confirms the possible existence of this two-way feedback. Furthermore, we have found that this feedback may be influenced by climate change. Compared the feedback between ENSO and ASO during two periods: 1984–2000 (P1) and 1984–2022 (P2), we found that the two-way feedback between ENSO and ASO has weakened during P2 compared to P1. This weakening may be attributed to changes in the Arctic Oscillation anomalies associated with ASO during P2, which led to a significant reduction in the relationship between ASO and North Pacific sea surface temperatures. In the future, if the relationship between ASO and the Arctic Oscillation strengthens again, this feedback loop could become more pronounced. In addition, we evaluated the capability of several CMIP6 models with high model top to simulate the feedback loop between ENSO and ASO. The findings reveal that, apart from the IPSL-CM6A-LR, most models fail to accurately reproduce this feedback. This may be one of the reasons for the significant discrepancies between the simulated and observed interannual variations in ENSO and ASO in the current CMIP6 models.

Keywords El Niño-Southern Oscillation · Arctic stratospheric ozone · Two-way feedback

1 Introduction

The El Niño-Southern Oscillation (ENSO) represents a principal driver of interannual variability in the global climate (Bjerknes 1969; Ropelewski and Halpert 1987; Bove et al. 1998; Alexander et al. 2002; McPhaden et al. 2006). Although ENSO originates in the tropical Pacific, it influences not only tropospheric weather and climate but also exerts a significant impact on stratospheric climate by altering atmospheric waves and circulation patterns (García-Herrera et al. 2006; Calvo et al. 2017; Domeisen et al. 2019; Rao and Ren 2016).Extensive research, based on observations and model simulations, has confirmed that ENSO can influence the stratospheric climate by altering wave activity and modifying wave fluxes entering the stratosphere, which impacts the strength of the Arctic stratospheric vortex and the Brewer-Dobson (BD) circulation (García-Herrera et al. 2006; Calvo et al. 2017; Domeisen et al. 2019; Xia et al. 2021b). Specifically, the El Niño signal (the warm phase of ENSO) propagates from the tropical Pacific to the polar stratosphere via atmospheric Rossby waves. During the Northern Hemisphere winter, the anomalous tropical sea surface temperatures (SST) associated with El Niño can deepen the Aleutian Low, which enhances the planetary waves entering the stratosphere (i.e., linear interference). The enhanced Rossby wave propagation in the stratosphere weakens the Arctic stratospheric vortex and strengthens the BD circulation (García-Herrera et al. 2006; Calvo et al. 2017; Domeisen et al. 2019). Conversely, La Niña (the cold

✉ Fei Xie
xiefei@bnu.edu.cn

✉ Yan Xia
xiayan@bnu.edu.cn

[1] Faculty of Geographical Science/School of System Science, Beijing Normal University, Beijing, China

[2] Frontiers Science Center for Deep Ocean Multispheres and Earth System (FDOMES)/Key Laboratory of Physical Oceanography/Institute for Advanced Ocean Studies, Ocean University of China, Qingdao, China

Published online: 09 January 2025

phase of ENSO) leads to a stronger Arctic stratospheric vortex, weakened BD circulation, and lower polar stratospheric temperatures (Iza et al. 2016).

Due to prevailing environmental conditions, the polar stratosphere largely lacks the capacity to produce substantial amounts of ozone, therefore, ozone distribution and variability in this region are primarily governed by meridional transport from the tropical stratosphere, the extent of mixing within polar regions, and local chemical depletion processes (Weber et al. 2011; Lubis et al. 2017; Hong and Reichler 2021; He et al. 2024). Given ENSO's ability to modulate both the stratospheric polar vortex and BD circulation, ENSO plays a crucial role in controlling the interannual variability of stratospheric ozone. Specifically, ENSO not only influences ozone concentrations in tropical and mid-latitude stratospheres but also significantly affects ASO variability (Brönnimann et al. 2004; Eyring et al. 2006; Cagnazzo et al. 2009; Lu et al. 2019; Xie et al. 2020; Niu et al. 2023). Brönnimann et al. (2004) did report the accumulation of unusually high total ozone columns over the Arctic and mid-latitudes during the strong and prolonged El Niño events of 1940–1942. Numerous studies have indicated that ozone changes in the lower tropical stratosphere are primarily driven by advection effects due to tropical upwelling anomalies (Calvo et al. 2010; Xie et al. 2014). While in the middle and high latitudes, stratospheric ozone changes associated with ENSO are produced by advection changes caused by BD circulation and horizontal mixing changes associated with polar vortex anomalies caused by Rossby wave breaking. During El Niño events, increased planetary wave flux into the Arctic stratosphere weakens the polar vortex. This weakening of the polar vortex enhances the stratospheric meridional circulation (BD circulation), transporting more tropical ozone from the source region to the Arctic. Additionally, the weakened polar vortex further enhances the horizontal mixing of ozone, both of which contribute to the increase in ASO concentration (Benito-Barca et al. 2022).

As a key component of the climate system, stratospheric ozone plays a crucial role not only in maintaining radiative balance and protecting the Earth from harmful solar ultraviolet radiation (Kerr and McElroy 1993; Chipperfield et al. 2015; Xia et al. 2018), but also in influencing stratospheric temperature and circulation through radiative heating. The behavior of the polar vortex is particularly sensitive to variations in stratospheric ozone, as changes in ozone distribution can modify the thermal structure of the stratosphere, influencing atmospheric circulation patterns. When the ozone layer is depleted, it can weaken the polar vortex, leading to its destabilization and splitting, which will significantly impact tropospheric weather and climate (e.g., Baldwin and Dunkerton 2001; Cagnazzo et al. 2009; Ineson and Scaife 2009; Thompson et al. 2011; Byrne and Shepherd 2018).

Since the concept of the "Antarctic ozone hole" was first introduced by British scientist Joe Farman and his colleagues in 1985 (Farman et al. 1985), the destruction of stratospheric ozone and its climatic impacts have drawn widespread attention. Although the multi-decadal depletion of Arctic stratospheric ozone (ASO) is far less pronounced than that of the Antarctic (Montzka et al. 2011), the interannual variability of ASO is comparable to, and even stronger than, that of the Antarctic (Montzka et al. 2011). Therefore, the climatic impact of ASO cannot be overlooked (Xia et al. 2021a). Smith and Polvani (2014) reported the impacts of extreme ASO depletion events on tropospheric circulation, precipitation, and surface temperature. Calvo et al. (2015), using the coupled global atmospheric model (WACCM4), demonstrated that ASO variations significantly impact mid- to high-latitude tropospheric circulation and sea level pressure (SLP) anomalies in the Northern Hemisphere, affecting tropospheric winds, temperature, and precipitation. Studies by Xie et al. (2018) and Ma et al. (2019) showed that ASO can influence precipitation in central China and northwestern North America. Hu et al. (2019) found that ASO depletion leads to increased humidity in the subtropics and shifts the northern boundary of the Hadley circulation toward the equator. Research by von der Gathen et al. (2021) revealed that climate warming will increase seasonal ozone loss in the Arctic, leading to greater variability in atmospheric and surface climate patterns. Friedel et al. (2022), through atmospheric chemistry model analysis, found that ASO depletion can significantly influence Northern Hemisphere climate modes, including warming over the Eurasian continent and increased dryness in central Europe, emphasizing the critical role of stratospheric ozone in regulating surface climate.

Beyond these impacts, Xie et al. (2016, 2017) also pointed out that ASO can significantly influence tropical SST. The radiative balance anomalies induced by ASO variations lead to abnormal stratospheric circulation, particularly affecting the dynamics of the polar vortex. Disturbances in the vortex initiate changes in stratosphere-troposphere coupling, which, through the downward control mechanism, affect large-scale atmospheric circulation patterns, such as the North Pacific Oscillation (NPO, Rogers 1981) patterns over the North Pacific. The NPO can modulate tropical SST through two pathways:

(1) The negative NPO anomaly and the induced positive Victoria mode (VM, Bond et al. 2003) can, through the seasonal footprinting mechanism (Vimont et al. 2001, 2003), significantly modulates tropical SST, with effects emerging approximately 20 months later (Alexander et al. 2010; Ding et al. 2015; Xie et al. 2016; Chen et al. 2018, 2024). (2) The other is by triggering the North Pacific Meridional Mode (NPMM, Chiang and Vimont 2004), which subsequently affects SST. NPO can trigger the NPMM through wind-evaporation-SST feedback (Xie 1999). The NPMM

propagates SST anomalies from the subtropics to the equator, initiating the development of ENSO events, a process that spans about one year (Chang et al. 2007; Zhang et al. 2009; Yu and Kim 2011; Larson and Kirtman 2013; Ding et al. 2022). These studies proposed a mechanism through which ASO variations influence ENSO via the high-latitude stratosphere-troposphere pathways and extratropical-tropical climate teleconnections, revealing the potential predictive value of ASO for ENSO.

As discussed above, ENSO and ASO are two key factors influencing weather and climate, and numerous studies have demonstrated the strong linkage between them. On the one hand, ENSO can substantially influence ASO variability; on the other hand, ASO variability can markedly impact the occurrence and development of ENSO. This suggests a potential bidirectional interaction or dynamic feedback between ASO and ENSO. However, previous studies have often focused on only one aspect, neglecting the integrated relationship between ENSO and ASO, which hampers accurate forecasting of their future evolution.

Therefore, this paper constructs the two-way feedback relationship between ENSO and ASO based on observational and reanalysis data, and we select 12 models from the CMIP6 historical experiments for validation, aiming to evaluate the models' simulation capabilities. The remainder of this paper is organized as follows: Sect. 2 provides a detailed description of the data and methods used in this study. Section 3 discusses the observed interactions between ENSO and ASO and proposes a potential two-way feedback loop. Section 4 analyzes the key mechanisms driving this two-way feedback and compares the simulation results from the 12 CMIP6 models. Finally, Sect. 5 summarizes and discusses the findings of the study.

2 Data and methods

2.1 Observational and reanalysis data

In this study, we selected the region of 60–90°N and 100–50 hPa, where ozone concentration changes and depletion are most significant in the Northern Hemisphere (Manney et al. 2011). The ASO index is defined as the monthly mean ozone concentration in this region, after removing the climatological seasonal cycle. The ENSO index is derived from the NINO3.4 index, compiled by the Climate Prediction Center of the National Oceanic and Atmospheric Administration (NOAA). To compare and validate the reliability of the results, we used one observational ozone dataset and two reanalysis ozone datasets, covering the period from January 1984 to December 2022.

The ozone observational data are from the Stratospheric Water and Ozone Satellite Homogenized (SWOOSH) dataset, while the reanalysis data are from the Japanese 55-year Reanalysis (JRA-55, Kobayashi et al. 2015) and the European Centre for Medium-Range Weather Forecasts (ECMWF) Fifth Generation Global Reanalysis dataset (ERA5). Among these datasets,

The SWOOSH database is a merged zonal-mean monthly-mean dataset which contains observations from the SAGE II (v7.0; Stratospheric Aerosol and Gas Experiment), SAGE III (v4), HALOE (v19; Halogen Occultation Experiment), UARS MLS (v5; Upper Atmosphere Research Satellite) and EOS Aura MLS (v4.2; Earth Observing System) instruments. In this study, we used version 2.6 of the SWOOSH dataset, which has a horizontal resolution of 2.5° latitude and a vertical resolution of 31 pressure levels from 1 to 316 hPa, covering the period from January 1984 to the present. We specifically used the "combinedo3q" product.

JRA-55 has a horizontal resolution of 2.5° × 2.5° and 37 pressure levels with the top at 1 hPa. In JRA-55, ozone observations are not assimilated directly. Before 1979, a monthly-mean climatology for the 1980–1984 period is used. From 1979 onwards, ozone fields are produced using an offline chemistry– climate model (MRI-CCM1; Meteorological Research Institute) that assimilates TCO observations from NASA's TOMS (Total Ozone Mapping Spectrometer) until 2004 and Aura OMI afterwards using a nudging scheme (Shibata et al. 2005).

ERA5 has a horizontal resolution of 0.5° × 0.5° and a vertical resolution spanning 37 pressure levels from 1000 to 1 hPa. The ozone data were assimilated through the ECMWF Integrated Forecasting System (IFS) by incorporating a range of observational data, ensuring high accuracy and consistency.

In addition to ozone data, SST and SLP data were obtained from the HadSST and HadSLP datasets, respectively, provided by the Hadley Centre for Climate Prediction and Research at the UK Met Office. Zonal wind (U), temperature (T), and other data were sourced from the ERA5 dataset.

2.2 CMIP6 historical experiment simulation data

To evaluate the models' capability to simulate the two-way feedback between ENSO and ASO, we selected 12 high-top models (models with a high model top) from the CMIP6 historical experiments that include ozone output. For each model, we selected the "r1i1p1f1" ensemble member and utilized the monthly mean temperature, wind, and surface temperature data from the atmospheric component (due to the unavailability of SST data in some models, we used surface temperature data as a substitute). Additionally, we used the monthly mean ozone data simulated by the atmospheric chemistry component. Detailed information about the selected models is provided in Table 1.

Table 1 12 CMIP6 models used in this study

CMIP6 Models	Institution	Top height (hPa)	Resolution (longitude/latitude)
CESM2-WACCM	NCAR	4.5×10^{-6}	288×192
EC-Earth3-AerChem	EC-Earth-Consortium	0.01	512×256
MRI-ESM2-0	MRI	0.01	320×160
UKESM1-1-LL UKESM1-0-LL	MOHC NERC NIMS-KMA NIWA	0.01	192×144
MPI-ESM-1-2-HAM	HAMMOZ-Consortium	0.01	192×96
CNRM-ESM2-1 CNRM-CM6-1	CNRM-CERFACS	0.01	128×256
IPSL-CM6A-LR IPSL-CM5A2-INCA	IPSL	0.01	96×96
E3SM-2-0	E3SM-Project	0.01	512×256
MPI-ESM1-2-LR	MPI	0.01	192×96

2.3 Statistical significance testing

We calculated the statistical significance of the correlation between two autocorrelated time series using the two-tailed Student's t-test and the effective number of degrees of freedom N^{eff}(Bretherton et al. 1999). For this study, N^{eff} was determined by the following approximate method:

$$\frac{1}{N^{\text{eff}}} \approx \frac{1}{N} + \frac{2}{N}\sum_{j=1}^{N}\frac{N-j}{N}\rho_{XX}(j)\rho_{YY}(j)$$

where N is the sample size, ρ_{XX} and ρ_{YY} are the autocorrelation coefficients of the two series X and Y, respectively, at time lag j.

2.4 Eliassen-palm (E-P) flux calculation

We evaluated the propagation of wave activity using the following formulas. The method of calculating the quasi-geostrophic two-dimensional Eliassen-Palm (E-P) flux was given by (Andrews et al. 2016), the meridional (F_y) and vertical (F_z) components of the E-P flux and the E-P flux divergence (D_F) are expressed as:

$$F_y = -\rho_0 a\cos\varphi\overline{u'v'}$$

$$F_z = -\rho_0 a\cos\varphi\frac{Rf}{HN^2}\overline{v'T'}$$

$$D_F = \frac{\nabla\cdot F}{\rho_0 a\cos\varphi} = \frac{\partial\left(F_y\cos\varphi\right)/a\cos\varphi\partial\varphi + \partial F_z/\partial z}{\rho_0 a\cos\varphi}$$

where ρ_0 is the density of air; φ is the latitude; a is the radius of the Earth; R is the gas constant; f is the Coriolis parameter; H is the atmospheric-scale altitude (km); u and v are the zonal and meridional components of the wind, respectively; and T nis the temperature. The overline denotes the zonal mean. Superscript symbols indicate deviations from the zonal mean.

3 Observed interactions between ENSO and ASO

Previous studies have shown that ENSO can influence Northern Hemisphere stratospheric ozone with a lag of 2–3 months (Brönnimann et al. 2004; Eyring et al. 2006; Cagnazzo et al. 2009), and Northern Hemisphere stratospheric ozone can, in turn, influence the occurrence and development of ENSO with a lag of 20 months (Xie et al. 2016), suggesting the potential two-way feedback loop between them. To establish the aforementioned loop, this study analyzed the lead-lag correlation between the ASO index and the ENSO index (Fig. 1). Figure 1a shows the lead-lag results between SWOOSH ozone and ENSO during the period 1984–2000 (P1). It can be observed that there is indeed a cyclic correlation between ENSO and ASO. When ENSO leads ASO by 3–4 months, the positive correlation coefficient is 0.28, significant above the 95% confidence level. When ENSO lags ASO by approximately 20 months, a negative correlation above the 95% confidence level is observed, with the correlation coefficient reaching − 0.52. Figure 1d, similar to Fig. 1a, but it shows the results for the period 1984–2022 (P2). Compared to P1, the lead-lag correlations between ENSO and ASO during P2 have significantly weakened. When ENSO precedes ASO, the maximum positive correlation is 0.13. When ENSO follows ASO, the maximum negative correlation drops to − 0.25, which is significantly lower than that observed in P1.

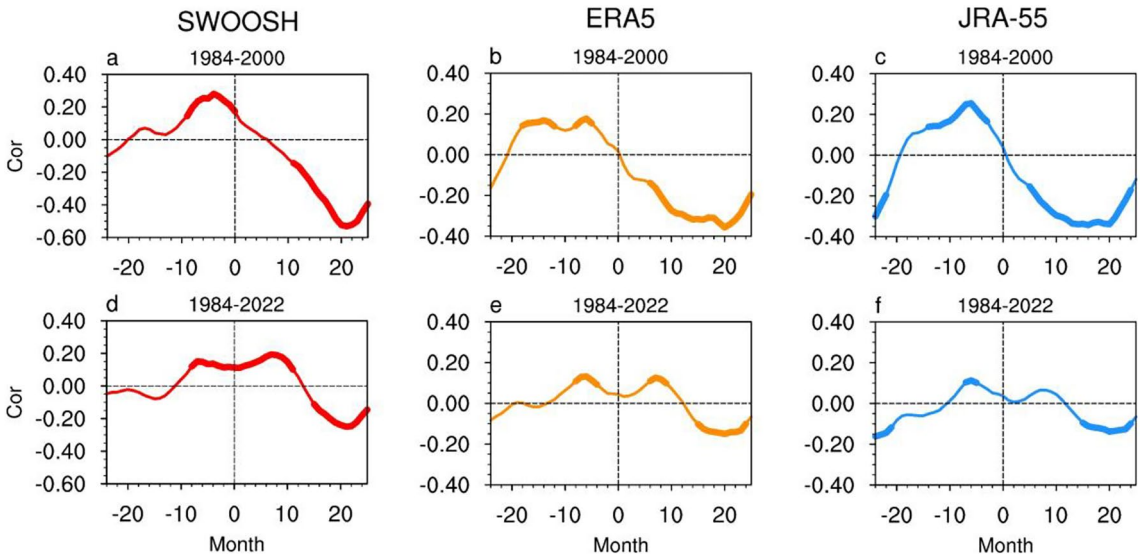

Fig. 1 Lead-lag correlation coefficients between the ASO and ENSO indices over different periods, based on three ozone datasets: SWOOSH (**a**, **d**), ERA5 (**b**, **e**), and JRA-55 (**c**, **f**). The top row corresponds to the period P1, and the bottom row represents the period P2. Positive values on the horizontal axis indicate that ASO precedes ENSO, while negative values indicate that ENSO precedes ASO. The bolded sections indicate correlation coefficients that pass the 95% significance test. The ENSO index is derived from the NINO3.4 index, compiled by NOAA's Climate Prediction Center

To improve the reliability of the results, this study repeated the above calculations using two reanalysis ozone datasets, ERA5 (Fig. 1b, e) and JRA-55 (Fig. 1c, f), alongside the ENSO index. The lead-lag correlations obtained from these two datasets are highly consistent with those from SWOOSH, indicating that the results are scarcely affected by the source of the ozone data and are thus reliable. This confirms the existence of a two-way cyclic feedback between ENSO and ASO, with a significant weakening of this feedback after 2000, which reflects clear interdecadal variability.

To better illustrate the variations of the lead-lag correlations between the ASO and ENSO indices before and after 2000, we constructed two aligned time series plots. Figure 2a shows the time series of the ASO and ENSO indices, with the time axis for ENSO shifted 4 months forward to represent the observed leading of ENSO. For 1984 to 2000, the correlation between the series is moderate, with a coefficient of 0.28. However, this correlation decrease significantly during 2000 to 2022, dropping to -0.10 and even becomes negative. Figure 2b shows these two series after ASO × − 1, with the time axis for ASO shifted 20 months forward to represent the observed lead of ASO. After ASO × − 1, the alignment between the sequences can be compared more intuitively. From 1984 to 2000, the two series match well, with a correlation coefficient of − 0.53. While for 2000–2022, the correlation weakens substantially, dropping to − 0.10. These results further support a significant change in this relationship around 2000.

Interrelated time series often exhibit similarities in their periodic distributions. To better compare the interdecadal changes in the relationship between ENSO and ASO, spectral analyses were conducted on the ASO and ENSO indices for P1 and P2 periods respectively (Fig. 2b–e). During P1, the ASO and ENSO time series show similar low-frequency spectra in the 1 to 6-year band (Fig. 2b, d), indicating a strong connection. However, during P2, the spectra of ASO and ENSO shows significant differences. These results further support the weakening relationship between ENSO and ASO after 2000.

The interdecadal variability in the cyclic feedback relationship between ENSO and ASO may stem from two underlying causes. On the one hand, numerous studies have demonstrated that the interaction between ENSO and the Arctic stratospheric polar vortex exhibits significant interdecadal variability. Over the past two decades, the influence of ENSO on the Arctic stratospheric polar vortex has markedly diminished or even become negligible (e.g., Chen and Wei 2009; Yu et al. 2015; Hu et al. 2017; Domeisen et al. 2019; Garfinkel et al. 2019; Zhang et al. 2022). One possible mechanism driving this change is climate change, which has modified low-frequency climate modes, such as the Pacific Decadal Oscillation (PDO) (Hu et al. 2018; Rao et al. 2019) and the Atlantic Multidecadal Oscillation (AMO). These low-frequency climate modes play an important modulating role in the pathway through which ENSO affects the Arctic stratospheric polar vortex (e.g., Feldstein 2002; Screen and Simmonds 2014). Since changes in the strength of the polar

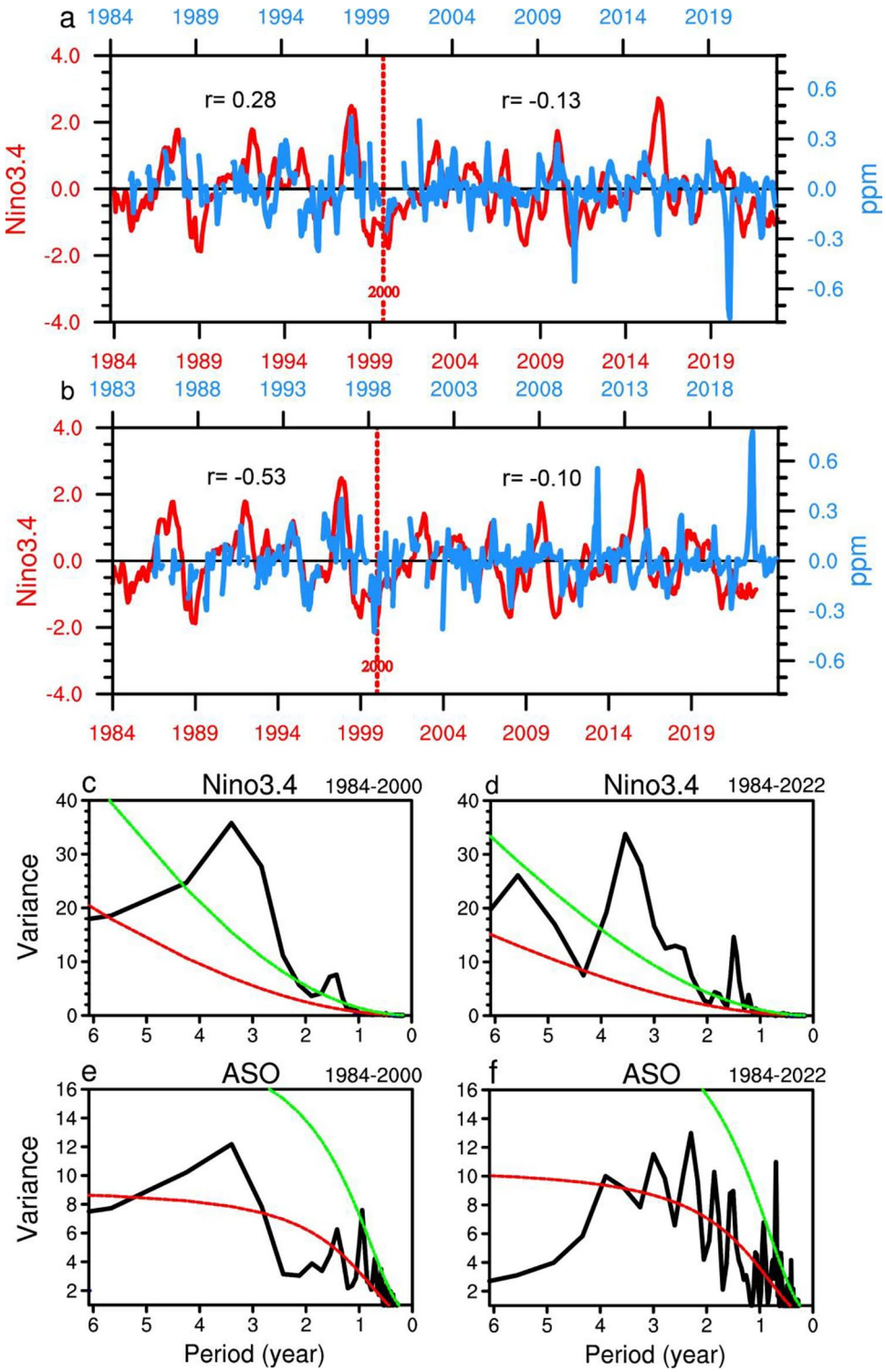

Fig. 2 **a** The time series of ASO index (blue line) and ENSO index (red line), with the ENSO time axis shifted 4 months forward. **b** The time series of ASO×− 1 index (blue line) and ENSO index, with the ASO time axis shifted 20 months forward. The year 2000 and the correlation coefficients of these two series before and after 2000 are marked in the corresponding positions in (**a**, **b**). The numbers labeled in (**a**, **b**) indicate that the maximum correlation between these two series during the corresponding period. **c** and **d** show the spectral analysis of the ENSO series for the periods P1 and P2, respectively. The black line denotes the spectral distribution, while the green and red lines represent the 95% confidence level and the red noise spectrum, respectively. **e** and **f** are the same as (**c**) and (**d**) but for the ASO index. The ozone data in (**a**, **b**) are from SWOOSH. Due to many missing values in the SWOOSH data, spectral analysis could not be performed; therefore, JRA-55 ozone data were used for Fig (**e**) and (**f**). The ENSO index is derived from the NINO3.4 index, compiled by NOAA's Climate Prediction Center

vortex induced by ENSO significantly contribute to the ASO concentration variability, the influence of ENSO on ASO also exhibits interdecadal variation. On the other hand, Wang et al. (2023) found that ASO influences North Pacific SST through its effects on the Arctic Oscillation. However, after 2000, the impact of ASO on North Pacific SST significantly weakened. This is attributed to two changes in the positive phase of the Arctic Oscillation: first, the positive geopotential height anomalies over high-latitude Asia weakened; second, abnormal westerlies in the mid-latitudes of the North Pacific will weaken the easterly anomalies over the North Pacific (He et al. 2022). These two changes significantly

weakened the relationship between ASO and North Pacific SST after 2000. Together, these studies provide two possible explanations for the significant weakening of the two-way feedback between ENSO and ASO after 2000.

Considering the interdecadal variability in the relationship between ENSO and ASO, this is why the study uses 2000 as a dividing line. We focus specifically on reconstructing the two-way feedback relationship between ENSO and ASO during P1. It is important to note that many studies have already discussed the possible mechanisms behind the significant weakening of their relationship after 2000 (e.g., Garfinkel et al. 2019; Zhang et al. 2022; Wang et al. (2023), and many others), therefore, the specific mechanisms of this change are not included in the scope of this paper's discussion.

4 The driving mechanisms of the two-way feedback between ENSO and ASO

4.1 ENSO's impact on ASO variability

It is noteworthy that due to the significant feedback loop between ENSO and ASO during P1, our study primarily focuses on the feedback loop during this period. Figure 3 shows the correlation distribution between ENSO and SLP (Fig. 3a) as well as zonal wind and temperature (Fig. 3b) respectively, with a one-month lag.

In the Indian Ocean and western Pacific regions, SLP positively correlates with the NINO3.4 index, while in the eastern Pacific and along the western coast of South America, SLP is negatively correlated with the NINO3.4 index (Fig. 3a). This correlation pattern is consistent with typical pressure characteristics during El Niño events, implying that the El Niño can signal deepens the Aleutian Low, which favorably interferes with the climatology quasi-stationary planetary wave pattern, increasing the planetary waves flux entering the stratosphere and thereby affecting the zonal wind and temperature in the Arctic stratosphere. Figure 3b shows that in the mid-latitudes, zonal wind negatively correlates with the NINO3.4 index, indicating westerly anomalies, while in the high latitudes, it positively correlates with temperature, indicating significant warm anomalies. These correlation distributions demonstrate that ENSO events can alter SLP and atmospheric circulation patterns.

Given that El Niño is strongest during the winter, which is around January. We use the January ENSO intensity as the basis for the composite analysis. To further analyze the impact of ENSO on ASO, we conducted a composite analysis of mean ozone concentration, zonal wind, temperature, and E-P flux during early spring (February–March, FM) for El Niño and La Niña events. Through lead-lag analysis, it can be observed that ENSO affects the ASO through atmospheric teleconnection mechanisms approximately 3–4 months in advance, so during FM, atmospheric wave activities can be observed, to explain the changes in ASO. To eliminate the interference from the Quasi-Biennial Oscillation (QBO), a linear regression method was used to remove the QBO signal from the time series before conducting the composite analysis. The analysis shows that during El Niño, ozone concentration in the Arctic stratosphere increases significantly, showing a positive ASO anomaly (Fig. 4a), which aligns with the characteristic changes in ASO during El Niño. Correspondingly, there is a significant increase in stratospheric temperature at high latitudes, accompanied by a weakening of the zonal wind (Fig. 4c). These changes in temperature and wind suggest that El Niño events enhance the transmission of E-P flux from the tropics to high latitudes

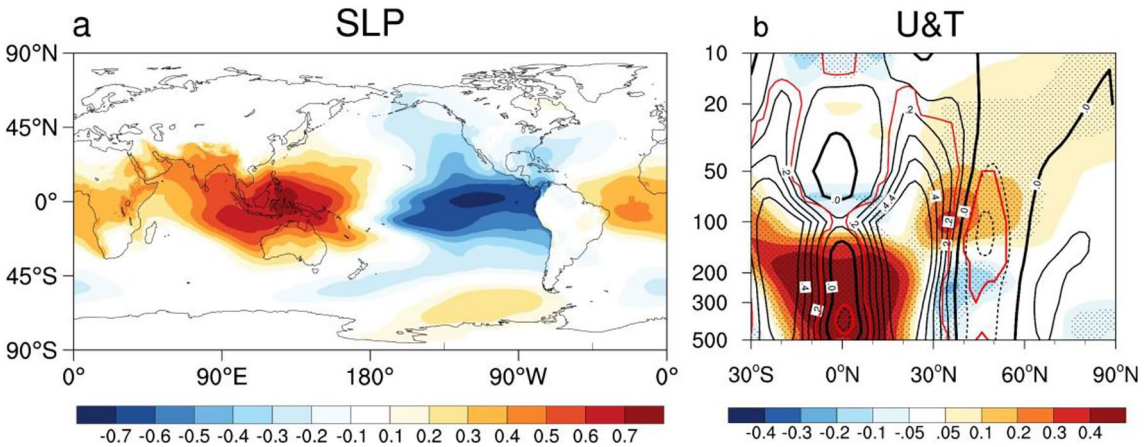

Fig. 3 During P1, the one-month lagged correlation distribution between the ENSO index and **a** SLP, and **b** zonal wind (U, black contours) and temperature (T, shaded). The contour interval is 0.1. Only areas passing the 95% significance test are shown in (**a**). Stippling and red contours in (**b**) indicate areas where the correlation with temperature and zonal wind passes the 95% significance test, respectively

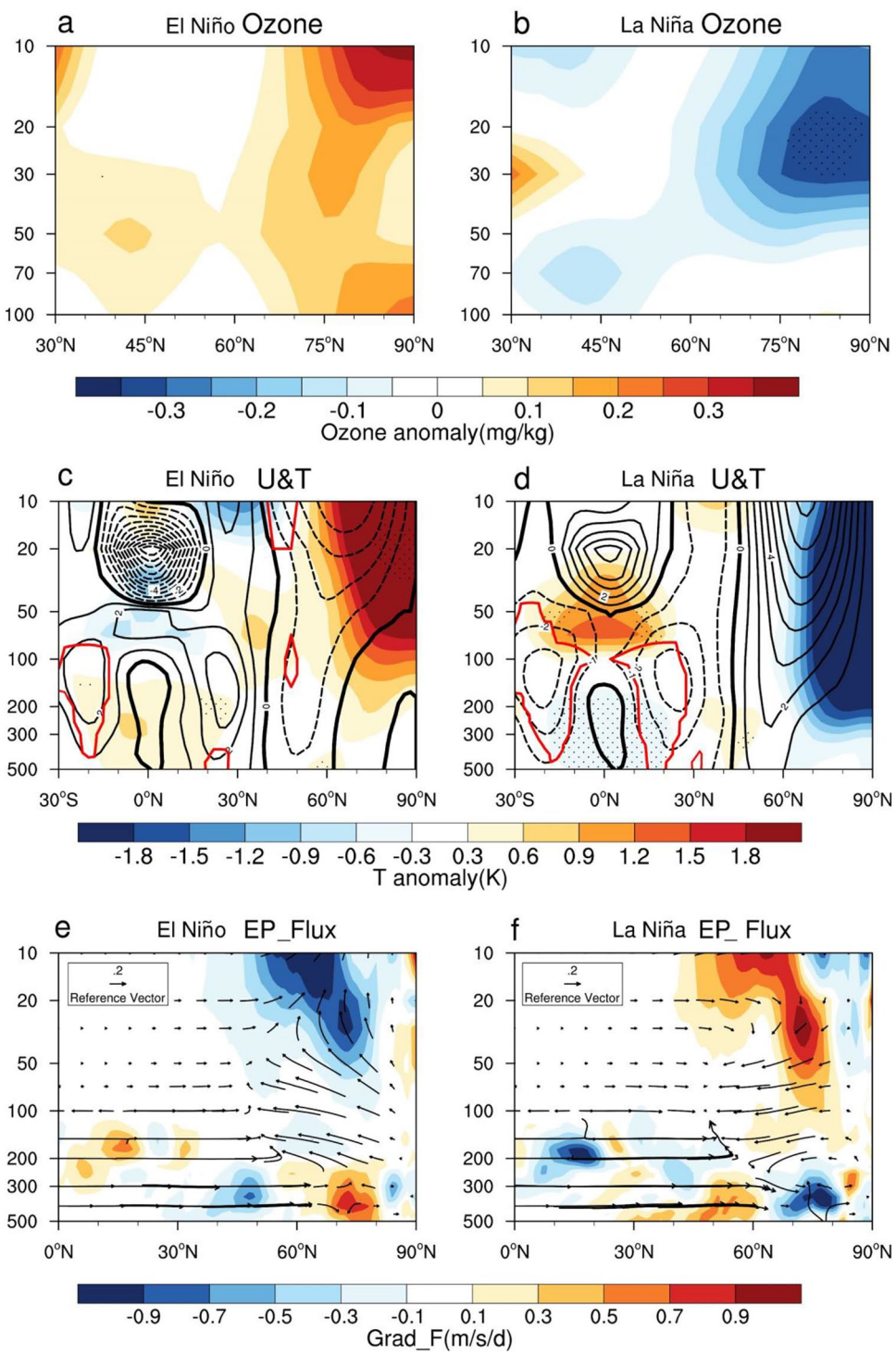

Fig. 4 After removing QBO events via linear regression, the composite distribution of FM-mean anomalies during P1 for **a**-**b** ozone (mg/kg), **c**–**d** U (black contours) and T (shaded), and **e**–**f** E-P flux anomalies (vectors, scaled by 10^{-4}) and divergence anomalies. These figures represent El Niño (left) and La Niña (right) events, respectively. Due to extensive missing data in SWOOSH, JRA-55 ozone data were used for Fig. 4a and b. The contour interval is 1 m/s. Stippling and red contours mark areas where the composite anomalies of ozone, temperature, and zonal wind pass the 95% significance test

(Fig. 4e) and cause convergence of wave activity in the high-latitude stratosphere. This leads to a weaker polar vortex, stronger BD circulation, and increased ozone transport from tropical regions to the poles. Concurrently, enhanced horizontal mixing of ozone due to wave breaking leads to a higher ASO concentration (Fig. 4a). In contrast, during La Niña, the ozone concentration in the Arctic stratosphere significantly decreases, showing a negative ASO anomaly (Fig. 4b), with a decrease in upper stratospheric temperature at high latitudes (Fig. 4d) and a strengthening of the zonal wind. These variations in temperature and wind suggest that La Niña events weaken wave activity, leading to downward divergence of E-P flux in the high-latitude stratosphere (Fig. 4f). The weakening of wave activity results in

a stronger polar vortex, weaker BD circulation, and reduced ozone transport from tropical regions to the poles. At the same time, weaker horizontal mixing of ozone leads to a decrease in ASO concentration.

Based on the above analysis, we have reconstructed the specific mechanism by which ENSO events alter stratospheric temperature and atmospheric circulation, affecting the transmission and divergence of E-P flux, thereby altering ASO concentration.

4.2 ASO modulates ENSO event

Following the mechanisms proposed by Xie et al. (2016) and Wang et al. (2023), which describe how ASO influences ENSO through a high-latitude stratosphere-troposphere pathway and extratropical-tropical teleconnection, we first reconstructed the pathway from ASO to SLP through the high-latitude stratosphere-troposphere route.

To better illustrate the correlation between ASO variability and SLP fields, we used the negative ASO values in our calculations. We found a significant correlation between ASO and the NPO (Fig. 5). The possible mechanism behind this correlation is that lower ASO concentrations reduce shortwave heating, thereby cooling the lower Arctic stratosphere, increasing the meridional temperature gradient, and strengthening the polar vortex. This strengthened stratospheric circulation can extend into the troposphere through coupling, triggering a positive Arctic Oscillation (AO) anomaly, accompanied by positive geopotential height anomalies over high-latitude Asia. These anomalies propagate eastward, affecting mid-latitude circulation over the North Pacific, leading to a negative NPO anomaly (Fig. 5).

Research indicates that negative NPO weakens the subtropical northeasterly trade winds, reducing evaporation in the northeastern subtropical Pacific and causing sea surface warming. This warming further weakens the trade winds, initiating a positive thermodynamic feedback between sea surface winds, evaporation, and temperature, known as the wind-evaporation-sea surface temperature (WES) feedback (Ding et al. 2022). Previous studies have proposed several pathways linking the NPO with tropical SST, the two most significant are: (1) The negative NPO influences surface heat flux and ocean temperature advection, resulting in a positive VM in SST. Xie et al. (2016) established an extratropical-tropical teleconnection based on the link between negative NPO and positive VM, and the VM's ability to modulate ENSO development via the seasonal footprinting mechanism (Chen et al. 2013; Ding et al. 2015). This teleconnection process spans approximately one and a half years. (2) In addition to the VM mode, the North Pacific Meridional Mode (NPMM) is another pathway through which the NPO influences ENSO variability. Studies have demonstrated that the NPO can trigger the wind-evaporation-sea surface temperature feedback in the northeastern subtropical Pacific, which in turn triggers the NPMM. The NPMM propagates SST anomalies from the subtropics to the equator, initiating the development of ENSO events, a process that spans about one year (Ding et al. 2022).

Given that ASO exhibits the greatest variability during winter, we use the November-December-January (NDJ) monthly mean ASO intensity (with December as a representative month) as the basis for the composite analysis. Figure 6 shows the composite analysis of SST fields lagging the November-December-January (NDJ) monthly mean ASO by different months. Using low ASO years (left column) as an example, when SST lags the winter ASO by 3 months (i.e., March SST field), a clear positive VM pattern emerges. The negative NPO signal is effectively linked to the positive VM anomaly (Fig. 6a). As positive VM evolves, it triggers westerly anomalies in the northeastern subtropical Pacific through the wind-evaporation-sea surface temperature feedback. These westerly anomalies, through air-sea interactions,

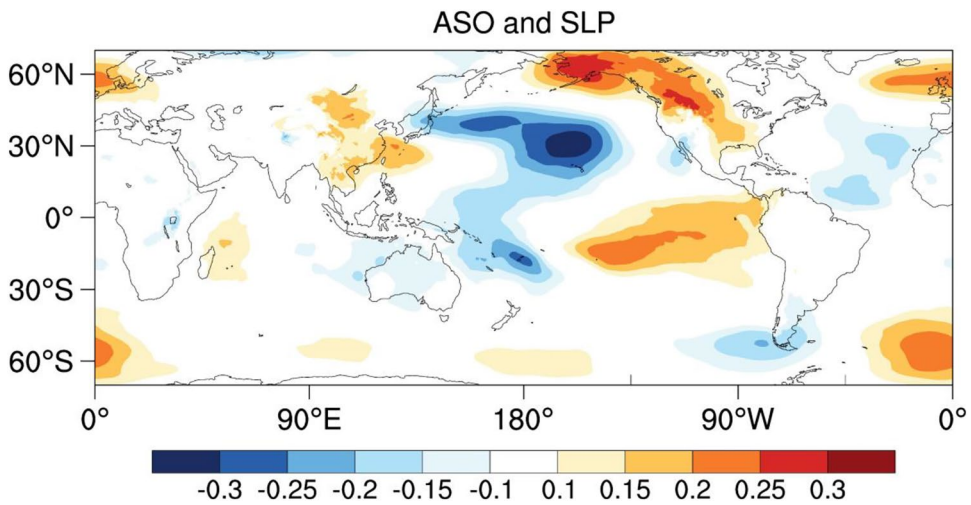

Fig. 5 The correlation distribution between ASO × − 1 and SLP during P1. Only areas passing the 95% significance test are shown. The ozone data are from SWOOSH

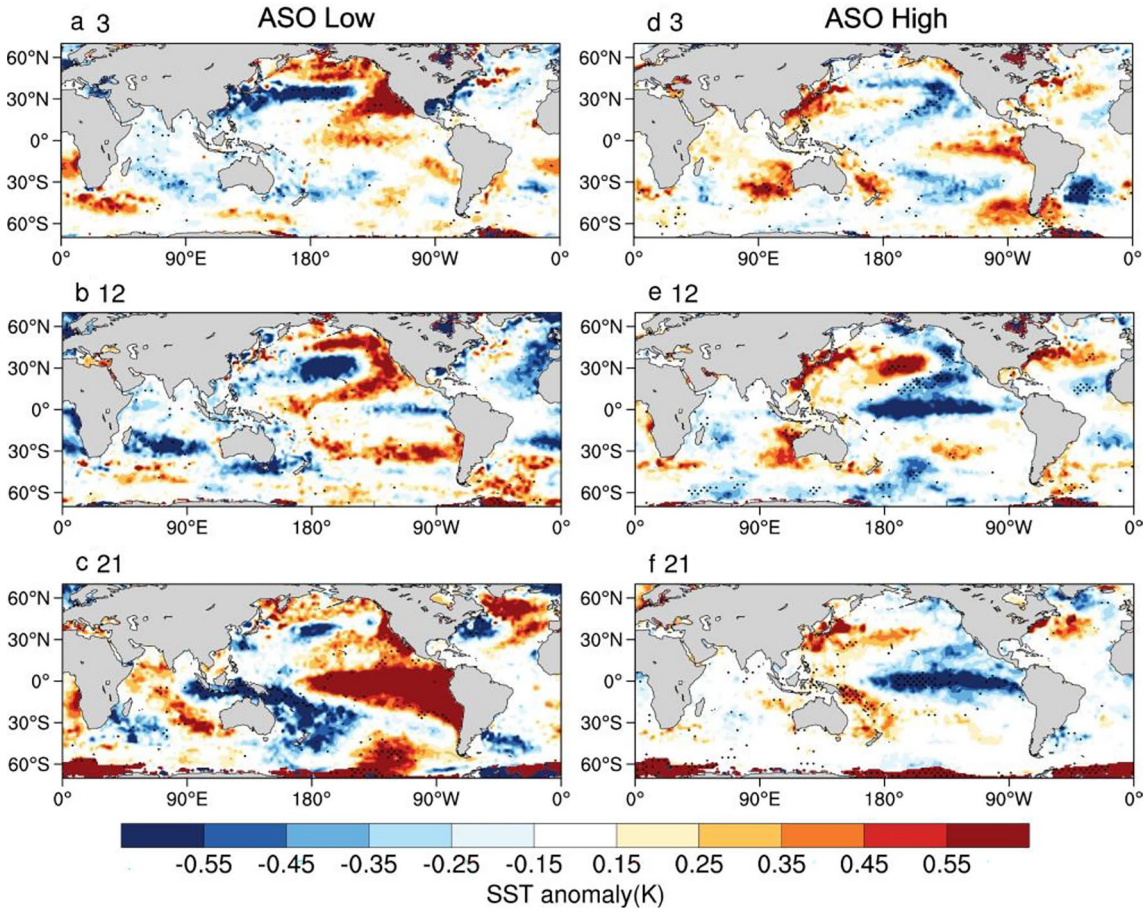

Fig. 6 Composite SST anomalies for NDJ monthly mean ASO leading SST by varying months in high and low ASO years during P1. **a** 3 months (March SST), **b** 12 months (December SST), and **c** 21 months for low ASO years. **d**–**f** correspond to the high ASO years. Stippling indicates areas passing the 95% significance test. Ozone is based on SWOOSH data, and SST data are from the HadSST dataset

alter the zonal SST gradient in the central-western tropical Pacific, which, in turn, trigger additional westerly anomalies, eventually leading to an El Niño event (Fig. 6c). Previous studies suggest that the NPO/VM leads ENSO by over a year and a half (Ding et al. 2015). The results for high and low ASO years exhibit symmetry. Thus, when ASO leads ENSO by about 20 months, they exhibit a significant negative correlation.

4.3 CMIP6 simulations of the two-way feedback between ASO and ENSO

In the previous sections, we identified the possible two-way feedback processes and mechanisms between ASO and ENSO using observational and reanalysis data. To further explore how well CMIP6 models capture the ASO-ENSO relationship, we selected 12 high-top models with ozone output from the CMIP6 historical experiments (see Table 1). For comparison with observational results, we selected the corresponding model data during P1 and calculated the ASO and NINO3.4 indices for each model. The remaining calculation methods were the same as those used in the observational analysis.

Figure 7 presents the ENSO-ASO correlation results for each of the 12 models. The results can be grouped into three categories: (1) Models that capture the two-way feedback loop, but with peak correlation occurring in different months than observed, such as IPSL-CM6A-LR, UKESM1-0-LL, IPSL-CM5A2-INCA, E3SM-2–0, UKESM1-1-LL, and CNRM-ESM2-1 (Fig. 7d–i); (2) Models whose simulated results are nearly opposite to the observational results, such as CESM2-WACCM, EC-Earth3-AerChem, and MPI-ESM1-2-LR (Fig. 7a–c); and (3) Models that fail to reproduce similar results, such as MRI-ESM2-0, CNRM-CM6-1, and MPI-ESM-1-2-HAM (Fig. 7i–l). Notably, almost no model could fully replicate the observed two-way feedback between ASO and ENSO, either in the shape of the correlation or the timing of the peak correlation. Moreover, the relationship depicted by the models is much weaker than observed.

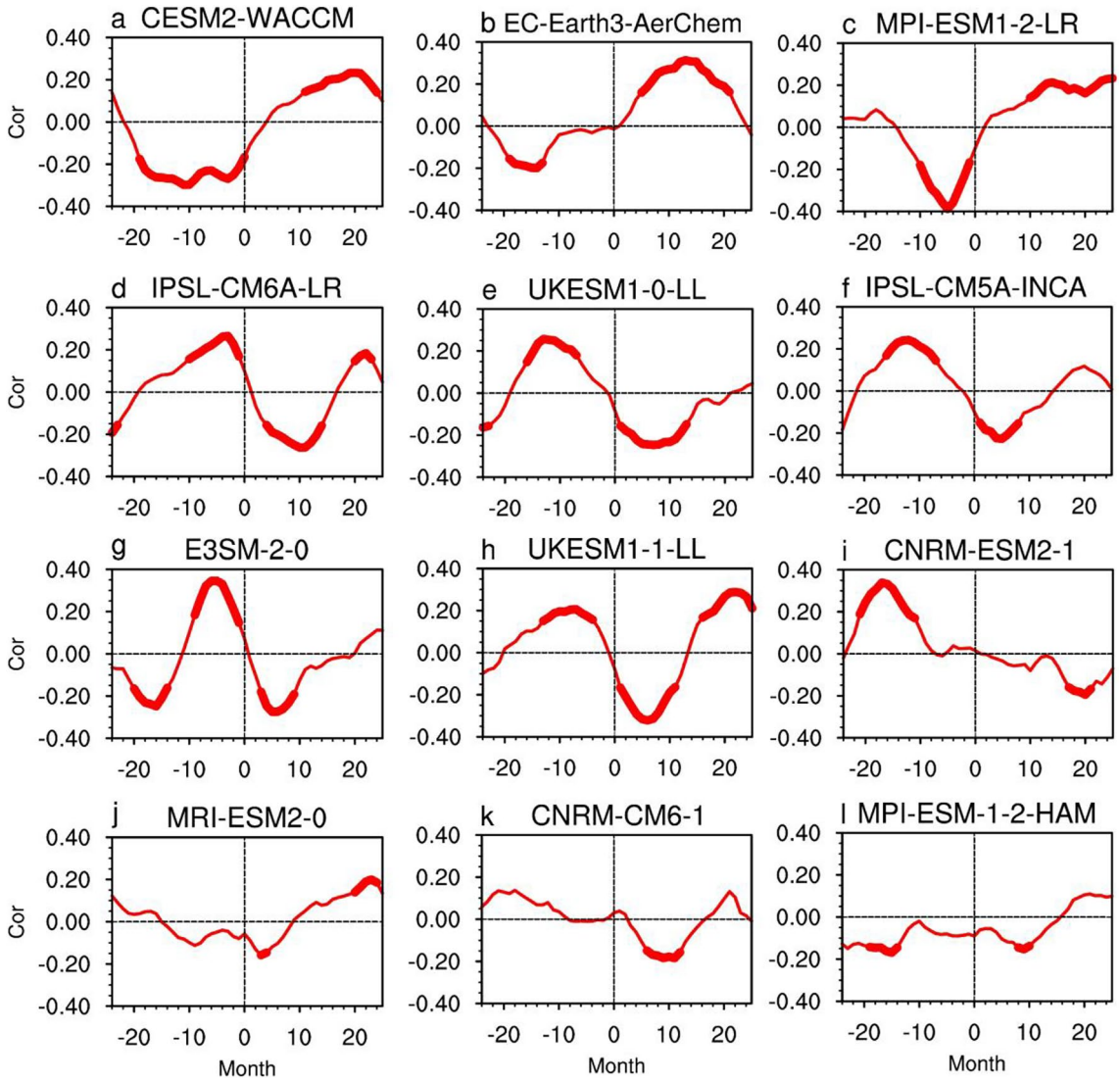

Fig. 7 Similar to Fig. 1, but based on the lead-lag correlation between ASO and ENSO indices during P1 from CMIP6 models. In the figures, positive values indicate ASO leading ENSO, while negative values indicate ENSO leading ASO. Model names are indicated above the corresponding subplots, and bold sections represent correlation results that pass the 95% significance test

Relatively speaking, models in the first category perform better, as they can capture the general patterns of the lead-lag relationships between ENSO and ASO (Fig. 7d–i). The common feature of the models in the first category is that, on one hand, when ENSO leads ASO by 4–12 months, the maximum positive correlation between these two occurs, taking longer than observed. On the other hand, when ASO leads ENSO by 6–10 months, the maximum negative correlation occurs, which is quicker than observed. Given the spatiotemporal complexity of atmospheric-oceanic processes, we believe that the temporal deviations in the above model results are related to the inability of these models to accurately simulate the ocean–atmosphere processes. Despite the discrepancies, the aforementioned model results still provide valuable insights.

Comparatively, the IPSL-CM6A-LR model (Fig. 7d) performed the best among the 12 models, successfully simulating ENSO influencing ASO with a 3-month lead time and a correlation coefficient of 0.265, almost identical to the observations. However, the simulation of ASO influencing ENSO occurred faster, with the highest correlation of − 0.26 when ASO led ENSO by about 10 months, which is lower than the observed result. When ASO leads ENSO by 20–24 months, the model shows a statistically significant positive correlation, contrary to the observed results.

To further explore the simulation of ENSO and ASO interactions in the IPSL-CM6A-LR model, we selected the key results from Figs. 4 and 6, which represent the main mechanisms identified in observational data, and replicated them in the model, as shown in Figs. 8 and 9. The results in

Fig. 8 are similar to those in Fig. 4, but the key difference is that during El Niño, the height of the maximum ASO anomaly in the model is lower than in the observations (Figs. 8a and 4a). The temperature anomaly location and values are also lower in the model compared to the observations. In the observations, the maximum warming at high latitudes occurs in the upper to middle stratosphere, with a temperature anomaly of 1.96 K (Fig. 4c). In the model, however, the maximum warming at high latitudes is in the lower to middle stratosphere, with a temperature anomaly of 1.47 K. Meanwhile, the maximum zonal wind anomaly in the model is 2.56 m/s (Fig. 8c), which is much smaller than the observed 4.37 m/s (Fig. 4c). As a result, the E-P flux transmission from the tropics to high latitudes is somewhat weaker in the model (Fig. 8e), but it still causes significant disturbances to the stratospheric circulation, weakening the polar vortex, strengthening the BD circulation, and increasing ASO concentration. Additionally, the model also simulates opposite conditions during La Niña compared to El Niño (Fig. 8b, d, f).

Figure 9 analysis shows that the IPSL-CM6A-LR model successfully simulates the pattern where, during low (/high) ASO years, the SST composite map, lagging NDJ monthly mean ASO by 3 months (March), shows positive (/negative) SST anomalies extending southwestward from the northeastern subtropical Pacific, resembling the positive (/negative) phase of NPMM (Fig. 9a/d). This phase maintains positive (/negative) SST anomalies for approximately two seasons, extending towards the equator (Fig. 9b/e) and eventually causing warming (/cooling) of the equatorial Pacific (Fig. 9c/f). This process involves an extratropical-tropical teleconnection, aligning with the previously discussed second pathway linking temperate NPO with tropical SST. Here, negative NPO triggers positive NPMM, propagating positive SST anomalies to the equatorial Pacific after two seasons, influencing El Niño events. We found that when ASO leads ENSO by 10 months, the strongest negative correlation occurs (Fig. 7d). This suggests that while the model can simulate the NPMM process, its duration is shorter than observed, indicating the need for further adjustment.

Figure 10 illustrates the two-way feedback relationship between ASO and ENSO established in this study to explain the dynamic evolution of their connection. Assuming that El Niño affecting ASO marks the beginning of the cycle, and given that El Niño is strongest during the winter, the entire cycle starts around January of the winter season. We denote the year when this feedback first develops as year (0), and the following years labeled sequentially as year (1), year (2), and so forth. Around February–March, El Niño induces an increase in ASO concentrations. After approximately 20 months, this elevated ASO concentration leads to a cooling of SST in the equatorial central-eastern Pacific, causing a La Niña event in year (2). This cycle continues to develop. The specific mechanisms are described as follows:

Step 1: An El Niño event in the tropical Pacific deepens the Aleutian Low, increasing wave flux into the Arctic stratosphere, weakening the polar vortex, and strengthening the BD circulation. Through this mechanism, the distant El Niño event increases ASO concentration after two to three months.

Step 2: The increase in ASO concentration absorbs more solar radiation, warming the lower Arctic stratosphere and weakening circulation. The weakened stratospheric circulation extends into the troposphere through coupling, triggering a negative Arctic Oscillation (AO) anomaly and a negative geopotential height anomaly over high-latitude Asia. These anomalies extend eastward, affecting mid-latitude circulation over the North Pacific, leading to a positive NPO anomaly. This results in a negative VM-like SST anomaly, which propagates to the tropical Pacific via the seasonal footprinting mechanism, eventually triggering a La Niña event under suitable conditions. This process takes more than a year and a half.

Step 3: The La Niña event subsequently decreases ASO concentration.

Step 4: The negative ASO anomaly then influences an El Niño event through the same mechanism.

5 Summary and discussion

This study, based on observational and reanalysis data, suggests that there may be a two-way feedback loop between ENSO and ASO. However, changes in the positive phase of the Arctic Oscillation associated with ASO have led to a weakening of this feedback since 2000. Amid global warming, as the positive phase of the AO associated with ASO strengthens, this potential two-way feedback loop may continue to influence the interannual variability of ENSO and ASO. We also evaluated the ability of several CMIP6 models to simulate the feedback processes between ENSO and ASO. We found that, except for the IPSL-CM6A-LR model performed well, most models failed to capture this feedback accurately. The MPI-ESM-1-2-HAM model performed the worst, failing to simulate the variations between ASO and ENSO. Overall, the results can be grouped into three categories: (1) models with simulated results nearly opposite to observational results; (2) models that capture the two-way feedback loop, but with peak correlation occurring in different months than observed; (3) models that almost entirely fail to reproduce similar results. In summary, nearly no model was able to fully replicate the observed two-way feedback between ASO and ENSO.

Harari et al. (2019) used the latest models from the Chemistry-Climate Model Initiative (CCMI) to simulate

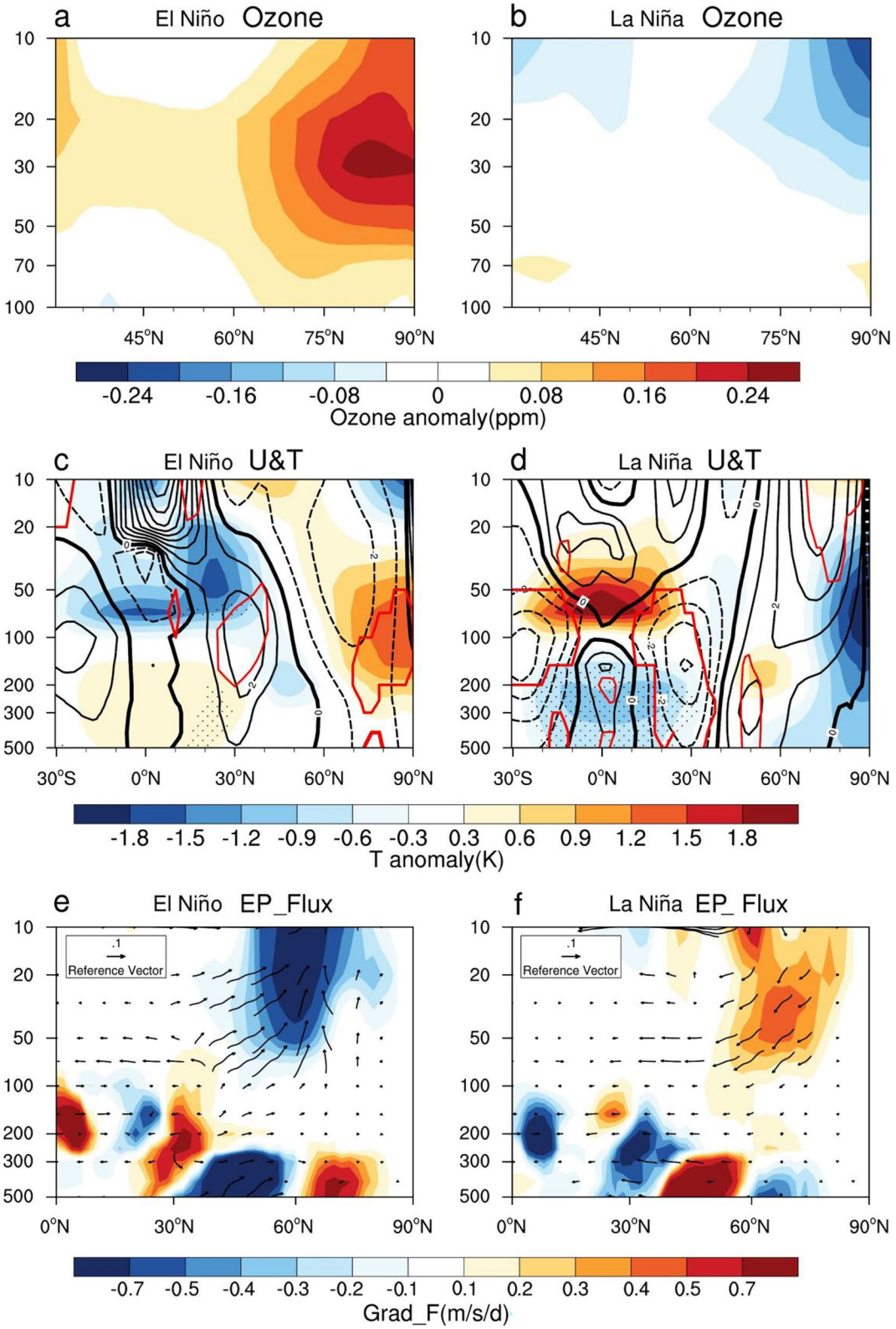

Fig. 8 Same as Fig. 4, but for the corresponding results from the IPSL-CM6A-LR model

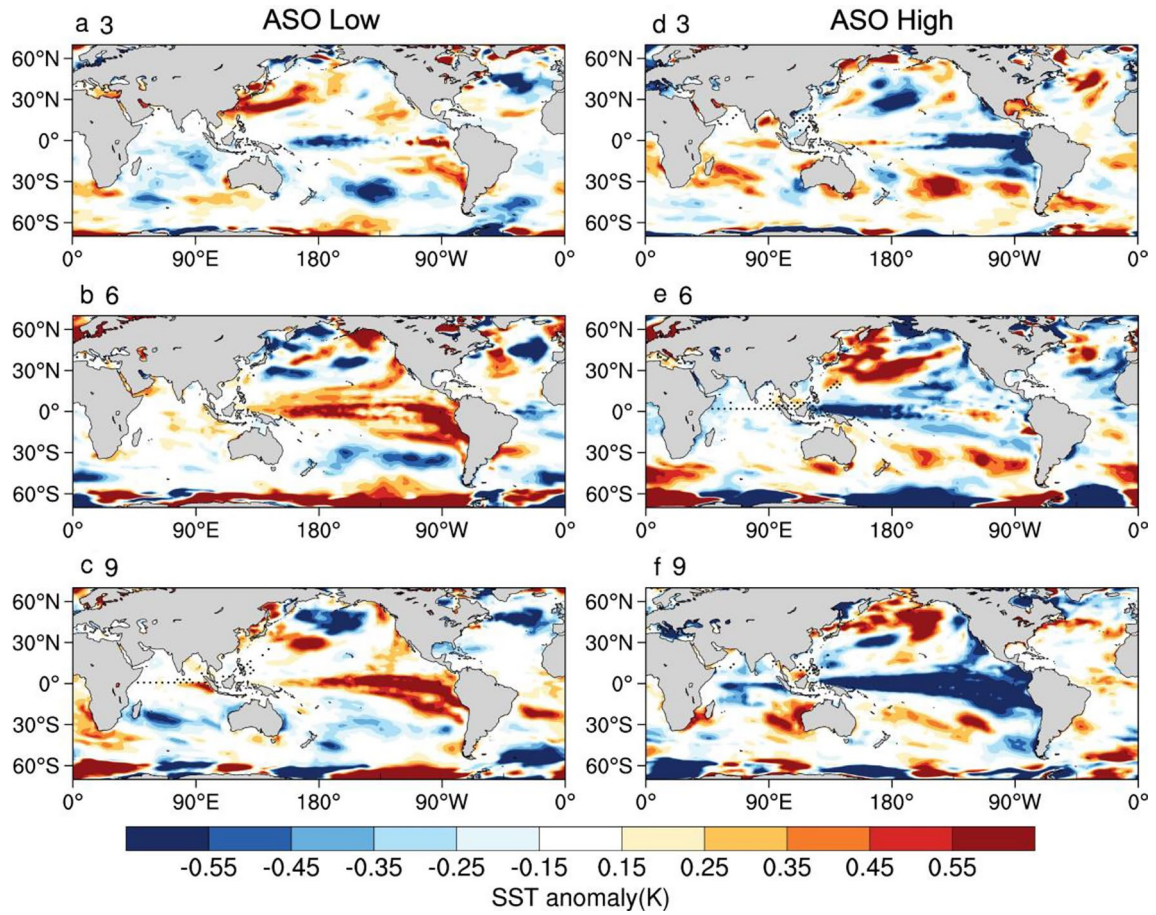

Fig. 9 Composite SST anomalies for low ASO years in the IPSL-CM6A-LR model, with NDJ mean ASO leading SST by **a** 3 months (i.e., March SST), **b** 6 months, and **c** 9 months. (Panels **d**–**f**) showing the same time lags, but correspond to high ASO years

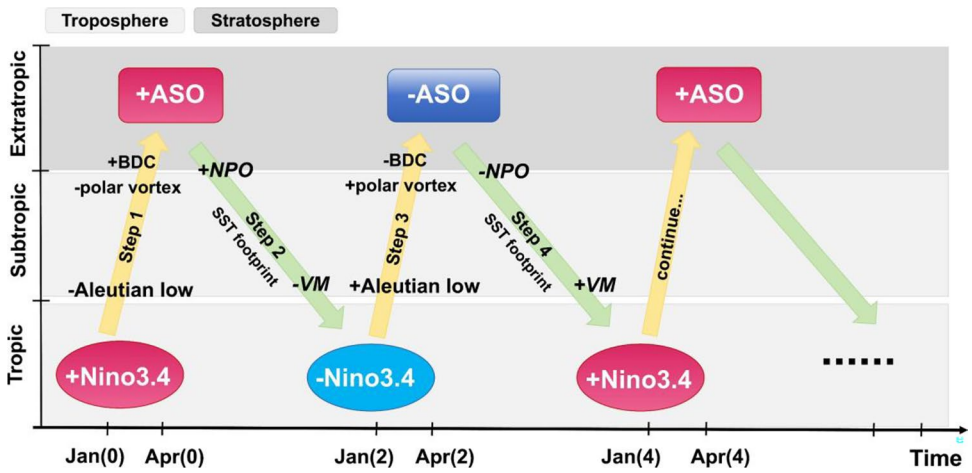

Fig. 10 Schematic diagram of the two-way feedback between ENSO and ASO. The red oval and blue oval correspond to El Niño and La Niña, respectively, while the red square and blue square correspond to ASO increase and decrease, respectively. The horizontal axis represents the temporal evolution, and the vertical axis represents different temperature zones. The light gray and dark gray backgrounds correspond to the troposphere and stratosphere, respectively

the two-way feedback between ENSO and ASO. Most CCMI models captured the correlation between ASO and stratospheric temperature, though a few performed slightly weaker than actual observations. However, the correlation between ASO and polar surface pressure was weak, while the correlation with polar 100 hPa geopotential height was strong, suggesting that ASO's influence on the troposphere primarily operates through the polar vortex. The study found no evidence of ASO's regulatory effect on ENSO in the CCMI models. Harari et al. (2019) suggested that

internal model variability and complex dynamic processes might be key factors affecting the simulation results. This study also found that the performance of the 12 models, along with their differences, suggests that most models may inadequately simulate the atmospheric and oceanic processes through which ENSO affects ASO and NPO affects ENSO, making it unlikely for this relationship to exist in most CMIP6 models. The reasons why most models cannot reproduce the possible feedback relationship between ENSO and ASO, as identified in observational data, need more detailed researches in the future. Models' ability to simulate interannual climate variability can be enhanced by addressing this issue.

ENSO can also influence Antarctic stratospheric ozone changes. While many studies have shown that Antarctic stratospheric ozone has a strong climate impact (e.g.Son et al. 2008; Gerber and Son 2014), no research indicates that it does significantly influence ENSO so far. This may be because the Southern Hemisphere is predominantly oceanic, lacking stable extratropical-tropical teleconnection pathways (Xie et al. 2016). Therefore, a two-way feedback loop between Antarctic stratospheric ozone and ENSO cannot be established.

Observational and reanalysis data both show a similar lead-lag relationship between ENSO and ASO, confirming its reliability. The poor performance of most CMIP6 models further highlights the difficulty in simulating this relationship, possibly due to their ability to capture ENSO's spatial pattern but not its variability. Establishing the two-way feedback between ENSO and ASO allows for a more systematic and accurate understanding of their connection, improves models' ability to simulate and predict ENSO, and enhances our capacity to respond to climate change amid global warming. However, several factors can influence this two-way feedback, and due to the nonlinear interactions among these factors, accurately predicting how this feedback will evolve in the future remains difficult. We will investigate this issue in greater depth in future work. While this study focuses on establishing the two-way feedback between ENSO and ASO, the broader framework and ideas presented here can be applied to various other issues in climate change research.

Acknowledgements This research has been made possible through the financial support of National Key Research and Development Program of China (No. 2022YFF0801701) and National Natural Science Foundation of China (Grants 42122037 and 42375070). We acknowledge SWOOSH、JRA-55、ECMWF and Hadley Centre for Climate Prediction and Research for their providing of the data.

Funding National Key Research and Development Program of China, 2022YFF0801701, Fei Xie, National Natural Science Foundation of China, 42122037, Fei Xie, 42375070, Fei Xie.

Data availability The authors declare that the datasets for this study are available in the following online repositories, The SWOOSH dataset is available at (https://www.esrl.noaa.gov/csd/groups/csd8/swoosh/). Data from the JRA-55 is freely available at (https://doi.org/https://doi.org/10.5065/D60G3H5B). The ERA5 reanalysis data can be downloaded from the ECMWF (https://cds.climate.copernicus.eu/cdsapp#!/home). The HadISST and HadSLP is available from the UK Met Office, (https://www.metoffice.gov.uk). The CMIP6 model data are available from the ESGF at (https://esgf-node.llnl.gov/search/cmip6/).

Declarations

Conflict of interest The authors declare that they have no known competing financial interests or personal relationships that could have appeared to influence the work reported in this paper.

References

Alexander MA, Bladé I, Newman M et al (2002) The atmospheric bridge: the influence of ENSO teleconnections on air-sea interaction over the global oceans. J Climate 15:2205–2231. https://doi.org/10.1175/1520-0442

Alexander MA, Vimont DJ, Chang P, Scott JD (2010) The impact of extratropical atmospheric variability on ENSO: testing the seasonal footprinting mechanism using coupled model experiments. J Climate 23(11):2885–2901. https://doi.org/10.1175/2010JCLI3205.1

Andrews DG, Leovy CB, Holton JR (2016) Middle Atmosphere Dynamics. Academic Press

Baldwin MP, Dunkerton TJ (2001) Stratospheric harbingers of anomalous weather regimes. Science 294:581–584. https://doi.org/10.1126/science.1063315

Benito-Barca S, Calvo N, Abalos M (2022) Driving mechanisms for the El Nino-Southern Oscillation impact on stratospheric ozone. Atmos Chem Phys 22:15729–15745. https://doi.org/10.5194/acp-22-15729-2022

Bjerknes J (1969) Atmospheric teleconnections from the equatorial pacific[1]. Mon Wea Rev 97:163–172. https://doi.org/10.1175/1520-0493(1969)097%3c0163:ATFTEP%3e2.3.CO;2

Bond NA, Overland JE, Spillane M, Stabeno P (2003) Recent shifts in the state of the north pacific. Geophys Res Lett 30:2183. https://doi.org/10.1029/2003GL018597

Bove MC, O'Brien JJ, Eisner JB et al (1998) Effect of El Niño on U.S. landfalling hurricanes. Revisited Bull Amer Meteor Soc 79:2477–2482. https://doi.org/10.1175/1520-0477(1998)079%3c2477:EOENOO%3e2.0.CO;2

Bretherton CS, Widmann M, Dymnikov VP et al (1999) The effective number of spatial degrees of freedom of a time-varying field. J Clim 12:1990–2009. https://doi.org/10.1175/1520-0442(1999)012%3c1990:TENOSD%3e2.0.CO;2

Brönnimann S, Luterbacher J, Staehelin J et al (2004) Extreme climate of the global troposphere and stratosphere in 1940–42 related to El Niño. Nature 431:971–974. https://doi.org/10.1038/nature02982

Byrne NJ, Shepherd TG (2018) Seasonal persistence of circulation anomalies in the southern hemisphere stratosphere and its implications for the troposphere. J Climate 31:3467–3483. https://doi.org/10.1175/JCLI-D-17-0557.1

Cagnazzo C, Manzini E, Calvo N et al (2009) Northern winter stratospheric temperature and ozone responses to ENSO inferred from an ensemble of chemistry climate models. Atmos Chem Phys 9:8935–8948. https://doi.org/10.5194/acp-9-8935-2009

Calvo N, Garcia RR, Randel WJ, Marsh DR (2010) Dynamical mechanism for the increase in tropical upwelling in the lowermost tropical stratosphere during warm ENSO events. J Atmos Sci 67:2331–2340. https://doi.org/10.1175/2010JAS3433.1

Calvo N, Polvani LM, Solomon S (2015) On the surface impact of Arctic stratospheric ozone extremes. Environ Res Lett 10:094003. https://doi.org/10.1088/1748-9326/10/9/094003

Calvo N, Iza M, Hurwitz MM et al (2017) Northern hemisphere stratospheric pathway of different El Niño flavors in stratosphere-resolving CMIP5 models. J Climate 30:4351–4371. https://doi.org/10.1175/JCLI-D-16-0132.1

Chang P, Zhang L, Saravanan R et al (2007) Pacific meridional mode and El Niño—Southern Oscillation. Geophys Res Lett. https://doi.org/10.1029/2007GL030302

Chen W, Wei K (2009) Interannual variability of the winter stratospheric polar vortex in the northern hemisphere and their relations to QBO and ENSO. Adv Atmos Sci 26:855–863. https://doi.org/10.1007/s00376-009-8168-6

Chen S, Chen W, Yu B, Graf H-F (2013) Modulation of the seasonal footprinting mechanism by the boreal spring Arctic oscillation. Geophys Res Lett 40:6384–6389. https://doi.org/10.1002/2013GL058628

Chen S, Yu B, Chen W, Wu R (2018) A review of atmosphere-ocean forcings outside the tropical pacific on the El Niño-Southern Oscillation occurrence. Atmosphere 9:439. https://doi.org/10.3390/atmos9110439

Chen S, Chen W, Xie S-P et al (2024) Strengthened impact of boreal winter north pacific oscillation on ENSO development in warming climate. npj Clim Atmos Sci 7:69. https://doi.org/10.1038/s41612-024-00615-3

Chiang JCH, Vimont DJ (2004) Analogous pacific and atlantic meridional modes of tropical atmosphere-ocean variability. J Climate. https://doi.org/10.1175/JCLI4953.1

Chipperfield MP, Dhomse SS, Feng W et al (2015) Quantifying the ozone and ultraviolet benefits already achieved by the montreal protocol. Nat Commun 6:7233. https://doi.org/10.1038/ncomms8233

Ding R, Li J, Tseng Y et al (2015) The victoria mode in the north pacific linking extratropical sea level pressure variations to ENSO. J Geophys Res: Atmospheres 120:27–45. https://doi.org/10.1002/2014JD022221

Ding R, Tseng Y-H, Di Lorenzo E et al (2022) Multi-year El Niño events tied to the North Pacific Oscillation. Nat Commun 13:3871. https://doi.org/10.1038/s41467-022-31516-9

Domeisen DIV, Garfinkel CI, Butler AH (2019) The teleconnection of El Niño Southern Oscillation to the stratosphere. Rev Geophys 57:5–47. https://doi.org/10.1029/2018RG000596

Eyring V, Butchart N, Waugh DW et al (2006) Assessment of temperature, trace species, and ozone in chemistry-climate model simulations of the recent past. J Geophys Res-Atmos 111:D22308. https://doi.org/10.1029/2006JD007327

Farman JC, Gardiner BG, Shanklin JD (1985) Large losses of total ozone in Antarctica reveal seasonal ClOJNOx interaction

Feldstein SB (2002) The recent trend and variance increase of the annular mode. J Climate 15:88–94. https://doi.org/10.1175/1520-0442(2002)015%3c0088:TRTAVI%3e2.0.CO;2

Friedel M, Chiodo G, Stenke A et al (2022) Springtime arctic ozone depletion forces northern hemisphere climate anomalies. Nat Geosci. https://doi.org/10.1038/s41561-022-00974-7

García-Herrera R, Calvo N, Garcia RR, Giorgetta MA (2006) Propagation of ENSO temperature signals into the middle atmosphere: a comparison of two general circulation models and ERA-40 reanalysis data. J Geophys Res. https://doi.org/10.1029/2005JD006061

Garfinkel CI, Schwartz C, Butler AH et al (2019) Weakening of the teleconnection from El Niño-Southern Oscillation to the Arctic stratosphere over the past few decades: what can Be learned from subseasonal forecast models? JGR Atmospheres 124:7683–7696. https://doi.org/10.1029/2018JD029961

Gerber EP, Son S-W (2014) Quantifying the summertime response of the austral jet stream and hadley cell to stratospheric ozone and greenhouse gases. J Clim 27:5538–5559. https://doi.org/10.1175/JCLI-D-13-00539.1

Harari O, Garfinkel C, Ziv SZ et al (2019) Influence of Arctic stratospheric ozone on surface climate in CCMI models. Atmos Chem Phys 19:9253–9268. https://doi.org/10.5194/acp-19-9253-2019

He Y, Zhu X, Sheng Z et al (2022) Observations of inertia gravity waves in the western pacific and their characteristic in the 2015/2016 Quasi-biennial oscillation disruption. J Geophys Res: Atmospheres 127:e2022JD037208. https://doi.org/10.1029/2022JD037208

He Y, Zhu X, Sheng Z, He M (2024) Identification of stratospheric disturbance information in China based on the round-trip intelligent sounding system. Atmos Chem Phys 24:3839–3856. https://doi.org/10.5194/acp-24-3839-2024

Hong H-J, Reichler T (2021) Local and remote response of ozone to Arctic stratospheric circulation extremes. Atmos Chem Phys 21:1159–1171. https://doi.org/10.5194/acp-21-1159-2021

Hu J, Li T, Xu H, Yang S (2017) Lessened response of boreal winter stratospheric polar vortex to El Niño in recent decades. Clim Dyn 49:263–278. https://doi.org/10.1007/s00382-016-3340-z

Hu J, Li T, Xu H (2018) Relationship between the north pacific gyre oscillation and the onset of stratospheric final warming in the northern hemisphere. Clim Dyn 51:3061–3075. https://doi.org/10.1007/s00382-017-4065-3

Hu D, Guan Z, Tian W (2019) Signatures of the Arctic stratospheric ozone in northern hadley circulation extent and subtropical precipitation. Geophys Res Lett 46:12340–12349. https://doi.org/10.1029/2019GL085292

Ineson S, Scaife AA (2009) The role of the stratosphere in the European climate response to El Niño. Nature Geosci 2:32–36. https://doi.org/10.1038/ngeo381

Iza M, Calvo N, Manzini E (2016) The stratospheric pathway of La Niña. J Clim 29:8899–8914. https://doi.org/10.1175/JCLI-D-16-0230.1

Kerr JB, McElroy CT (1993) Evidence for large upward trends of ultraviolet-b radiation linked to ozone depletion. Science 262:1032–1034. https://doi.org/10.1126/science.262.5136.1032

Kobayashi S, Ota Y, Harada Y et al (2015) The JRA-55 reanalysis: general specifications and basic characteristics. J Meteorol Soc Jpn 93:5–48. https://doi.org/10.2151/jmsj.2015-001

Larson S, Kirtman B (2013) The pacific meridional mode as a trigger for ENSO in a high-resolution coupled model. Geophys Res Lett 40:3189–3194. https://doi.org/10.1002/grl.50571

Lu J, Xie F, Tian W et al (2019) Interannual variations in lower stratospheric ozone during the period 1984–2016. J Geophys Res-Atmos 124:8225–8241. https://doi.org/10.1029/2019JD030396

Lubis SW, Silverman V, Matthes K et al (2017) How does downward planetary wave coupling affect polar stratospheric ozone in the Arctic winter stratosphere? Atmos Chem Phys 17:2437–2458. https://doi.org/10.5194/acp-17-2437-2017

Ma X, Xie F, Li J et al (2019) Effects of Arctic stratospheric ozone changes on spring precipitation in the northwestern united states. Atmos Chem Phys 19:861–875. https://doi.org/10.5194/acp-19-861-2019

Manney GL, Santee ML, Rex M et al (2011) Unprecedented Arctic ozone loss in 2011. Nature 478:469-U65. https://doi.org/10.1038/nature10556

McPhaden MJ, Zebiak SE, Glantz MH (2006) ENSO as an integrating concept in earth science. Science 314:1740–1745. https://doi.org/10.1126/science.1132588

Montzka SA, Reimann S, Engel A, et al (2011) Scientific Assessment of Ozone Depletion: 2010. Global Ozone Research and Monitoring Project - Report No 51

Niu Y, Xie F, Wu S (2023) ENSO modoki impacts on the interannual variations of spring Antarctic stratospheric ozone. J Clim 36:5641–5658. https://doi.org/10.1175/JCLI-D-22-0826.1

Rao J, Ren R (2016) Asymmetry and nonlinearity of the influence of ENSO on the northern winter stratosphere: 1. Observations JGR Atmospheres 121:9000–9016. https://doi.org/10.1002/2015JD024520

Rao J, Ren R, Xia X et al (2019) Combined impact of El Niño-Southern Oscillation and pacific decadal oscillation on the northern winter stratosphere. Atmosphere 10:211. https://doi.org/10.3390/atmos10040211

Rogers JC (1981) The north pacific oscillation. J Climatol 1:39–57. https://doi.org/10.1002/joc.3370010106

Ropelewski CF, Halpert MS (1987) Global and regional scale precipitation patterns associated with the El Niño/Southern oscillation. Mon Wea Rev 115:1606–1626. https://doi.org/10.1175/1520-0493(1987)115%3c1606:GARSPP%3e2.0.CO;2

Screen JA, Simmonds I (2014) Amplified mid-latitude planetary waves favour particular regional weather extremes. Nature Clim Change 4:704–709. https://doi.org/10.1038/nclimate2271

Shibata K, Deushi M, Sekiyama TT, Yoshimura H (2005) Development of an MRI chemical transport model for the study of stratospheric chemistry. Pap Met Geophys 55:75–119. https://doi.org/10.2467/mripapers.55.75

Smith KL, Polvani LM (2014) The surface impacts of Arctic stratospheric ozone anomalies. Environ Res Lett 9:074015. https://doi.org/10.1088/1748-9326/9/7/074015

Son S-W, Polvani LM, Waugh DW et al (2008) The impact of stratospheric ozone recovery on the southern hemisphere westerly jet. Science. https://doi.org/10.1126/science.1155939

Thompson DWJ, Solomon S, Kushner PJ et al (2011) Signatures of the Antarctic ozone hole in southern hemisphere surface climate change. Nature Geosci 4:741–749. https://doi.org/10.1038/ngeo1296

Vimont DJ, Battisti DS, Hirst AC (2001) Footprinting: a seasonal connection between the tropics and mid-latitudes. Geophys Res Lett 28:3923–3926. https://doi.org/10.1029/2001GL013435

Vimont DJ, Wallace JM, Battisti DS (2003) The Seasonal Footprinting Mechanism in the Pacific: Implications for ENSO

von der Gathen P, Kivi R, Wohltmann I et al (2021) Climate change favours large seasonal loss of Arctic ozone. Nat Commun 12:3886. https://doi.org/10.1038/s41467-021-24089-6

Wang T, Tian W, Lin Y et al (2023) Decadal changes in the relationship between Arctic stratospheric ozone and sea surface temperatures in the North Pacific. Atmos Res 292:106870. https://doi.org/10.1016/j.atmosres.2023.106870

Weber M, Dikty S, Burrows JP et al (2011) The Brewer-Dobson circulation and total ozone from seasonal to decadal time scales. Atmos Chem Phys 11:11221–11235. https://doi.org/10.5194/acp-11-11221-2011

Xia Y, Hu Y, Huang Y et al (2021) Significant contribution of severe ozone loss to the siberian-arctic surface warming in spring 2020. Geophys Res Lett 48:e2021GL92509. https://doi.org/10.1029/2021GL092509

Xia Y, Hu Y, Zhang J et al (2021b) Record arctic ozone loss in spring 2020 is likely caused by north pacific warm sea surface temperature anomalies. Adv Atmos Sci 38:1723–1736. https://doi.org/10.1007/s00376-021-0359-9

Xia Y, Huang Y, Hu Y On the Climate Impacts of Upper Tropospheric and Lower Stratospheric Ozone. Journal of Geophysical Research

Xie F, Li J, Tian W et al (2014) The relative impacts of El Nino Modoki, canonical El Nino, and QBO on tropical ozone changes since the 1980s. Environ Res Lett 9:064020. https://doi.org/10.1088/1748-9326/9/6/064020

Xie F, Li J, Tian W et al (2016) A connection from Arctic stratospheric ozone to El Niño-Southern oscillation. Environ Res Lett 11:124026. https://doi.org/10.1088/1748-9326/11/12/124026

Xie F, Zhang J, Sang W et al (2017) Delayed effect of Arctic stratospheric ozone on tropical rainfall. Atmos Sci Lett 18:409–416. https://doi.org/10.1002/asl.783

Xie F, Ma X, Li J et al (2018) An advanced impact of Arctic stratospheric ozone changes on spring precipitation in China. Clim Dyn 51:4029–4041. https://doi.org/10.1007/s00382-018-4402-1

Xie F, Zhang J, Li X et al (2020) Independent and joint influences of eastern Pacific El Nino-southern oscillation and quasi-biennial oscillation on Northern Hemispheric stratospheric ozone. Int J Climatol 40:5289–5307. https://doi.org/10.1002/joc.6519

Xie S-P (1999) A Dynamic Ocean–Atmosphere Model of the Tropical Atlantic Decadal Variability

Yu J-Y, Kim ST (2011) Relationships between extratropical sea level pressure variations and the central pacific and eastern pacific types of ENSO. J Climate. https://doi.org/10.1175/2010JCLI3688.1

Yu Y, Ren R, Cai M (2015) Dynamic linkage between cold air outbreaks and intensity variations of the meridional mass circulation. J Atmos Sci 72:3214–3232. https://doi.org/10.1175/JAS-D-14-0390.1

Zhang L, Chang P, Ji L (2009) Linking the pacific meridional mode to ENSO: coupled model analysis. J Climate. https://doi.org/10.1175/2008JCLI2473.1

Zhang R, Zhou W, Tian W et al (2022) Changes in the relationship between ENSO and the winter Arctic stratospheric polar vortex in recent decades. J Clim 35:5399–5414. https://doi.org/10.1175/JCLI-D-21-0924.1